LANGMUIR Article
Cite This: Langmuir 2019, 35, 3194−3203
pubs.acs.org/Langmuir

Bubble Dislodgment in a Capillary Network with Microscopic Multichannels and Multibifurcation Features

Cong Chao,[†] Xiaoqiang Jin,[†] Lijun Teng,[‡] Adam A. Stokes,[‡] and Xianfeng Fan*[,†]

[†]Institute for Materials and Processes, School of Engineering, The University of Edinburgh, The King's Buildings, Robert Stevenson Road, Edinburgh EH9 3FB, U.K.

[‡]Institute for Integrated Micro and Nano Systems, School of Engineering, The University of Edinburgh, The King's Buildings, Alexander Crum Brown Road, Edinburgh EH9 3FB, U.K.

Supporting Information

ABSTRACT: Bubble lodgment in a complex capillary network is a common issue in many industrial and biological processes. Research work reported in the literature only investigated bubble dislodgment in single channels and did not consider the effect of network complexity on the dislodgment. This paper focuses on the pressure required to dislodge single bubbles from a microscopic capillary network and investigates the factors affecting the dislodging pressure to facilitate the precise control of bubble flows in porous media. A capillary network with multibifurcation and a smoothly changed diameter is designed to closely mimic the structure of the physiological vascular networks. Over 600 bubble dislodgment experiments have been conducted to understand the effect of the network structure, channel dimensions, and bubble length on the dislodging pressure. The results indicate that the network structure is a dominant factor affecting the dislodging pressure that increases with the increase in network complexity. The effect of bubble length on the dislodging pressure depends on the bubble length. When the bubble length is less than a certain value, which is around 2 mm in this study, the dislodging pressure increases significantly with the decrease of bubble length. When the bubble length is larger than 2 mm, the dislodging pressure is independent of the bubble length. A model has been proposed to explain the bubble dislodgment in complex capillary networks. The impact of the network structure on the bubble dislodging pressure is characterized by a parameter c_j. The model indicates that the dislodging pressure is the function of bubble length, channel dimension, and network structure. The analysis of model parameters NB_j and MA_j shows that parameter c_j, rather than the channel size, dominates the dislodging pressure for bubbles with a length greater than 2 mm, and the increase rate of the dislodging pressure is significantly affected by both channel size and parameter c_j.

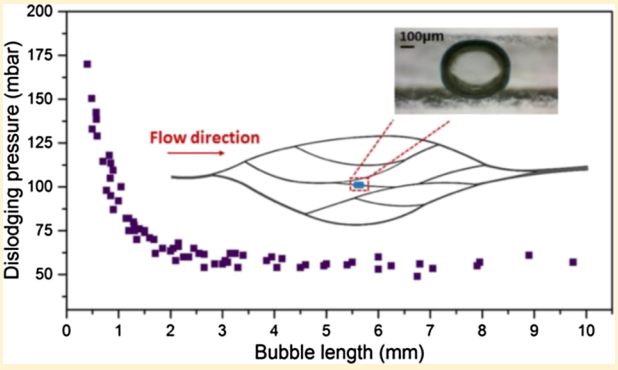

INTRODUCTION

Understanding of bubble flows in porous media is of particular interest in enhanced oil recovery,[1] intravascular gas embolism treatment,[2,3] fuel cells,[4−6] chemical reactors,[7,8] etc. For example, the infusion of bubbles into liquid can promote the mass or heat transfer in porous media, whereas bubbles may block the microchannel, thus disturbing the performance and reducing the efficiency of the fluid transport and migration in microfluidics. In medical applications, embolotherapy, a potential cancer treatment, utilizes bubble lodgment to achieve the occlusion of the arteriole or capillary in targeted sites. The lodged bubbles block microvessels to restrict blood supply to tumors and thus control the growth of tumor cells.[2,9−11] Another potential cancer treatment-microbubble-loaded drug delivery has been investigated for decades, while the safety issues still hinder its transform from bench to clinics.[12] The precise control of bubble lodgment at the targeted sites will significantly increase the therapeutic efficacy of treatment and decrease the side effects, such as the drug accumulation and distribution in healthy tissues. A thorough understanding of bubble lodgment and dislodgment in a complex capillary network helps to control the bubble flow in blood vessels and to improve the feasibility and efficiency of transport, for example, understanding where the bubble ultimately lodges, whether the bubble can be lodged and dislodged properly, and the persistence time of microbubbles lodged around the targeted sites.[13]

Bubbles flow as tubular bubbles in small blood vessels and may be lodged in capillaries, as observed in vitro by Calderón et al.[14] and in vivo by Samuel et al.[11] Samuel et al. observed that the perfluorocarbon bubbles with an average length of 76 ± 23 μm are often lodged at the capillary bifurcation in the

Received: October 1, 2018
Revised: December 14, 2018
Published: February 5, 2019

DOI: 10.1021/acs.langmuir.8b03323
Langmuir 2019, 35, 3194−3203

rats. In a bifurcation model patterned on poly(dimethyl siloxane), Calderón et al. found that the air bubble is commonly lodged at the daughter channel of the bifurcation. They also investigated the impact of bubble size, parent to daughter channel ratio, and cross-sectional shape and area on the bubble lodgment. The two groups also observed that the driving pressure required to dislodge the bubble is much higher than the lodging pressure. In order to precisely control the bubble flow in a capillary network, it is worth to investigate the pressure required to dislodge the bubble and the factors affecting the bubble dislodgment in a capillary network.

Some work has been done to investigate the bubble dislodgment in single microchannels. Blackmore et al. studied the bubble adhesion and detachment experimentally between two parallel plates with a width of 11 mm and a thickness of 30−200 μm and demonstrated the effect of D_c/h (where D_c is the bubble contact diameter and h is the channel height) on the capillary number required to detach a bubble.[15] They found that the shearing force required to dislodge a bubble decreased with the increase of bubble contact length. The liquid they used was engine oil and the channel surface was hydrophobic. As the channel width in their study was 11 mm in diameter, bubble flow condition and bubble dislodgment may be significantly different from that in the microscopic capillary network. Mohammadi and Sharp modeled the pressure difference required to dislodge "dry" bubbles in straight microchannels with a height and width of around 980 μm.[16] However, in their modeling, the drag force and viscous force were neglected, and the pinning force was assumed as the only resistant force acting on "dry" bubbles, which may not reflect the real flow conditions and the forces applied on the bubble in capillary networks. In addition, surface tension of the liquid[17] and channel surface properties (roughness and chemical heterogeneities[18]) should affect the bubble dislodgment in microchannels but were not taken into account in their modeling.

Few studies were performed to investigate bubble dislodgment in a complex capillary network. The network structures reported in the literature studies for the investigation into the bubble flow behavior are mainly single straight channels[6,13,16] and Y-type or U-type channels.[3,19−21] A single channel cannot simulate the flow conditions of bubble lodgment in a complex capillary network. For example, when an elongated bubble lodges in a single cylindrical channel, the pressure difference between the two ends of the bubble is the driving force to push the bubble, as there is no other pathway for the liquid to move forward. However, a capillary network has many bifurcations. Fluids in a network have several paths to choose and will consciously travel to the channel with smaller resistance (without bubbles/with less bubbles). In this case, the bubble will be more difficult to dislodge. The capillary network with multibifurcation is able to demonstrate the effect of multichannels and bifurcations on the flow resistance and bubble dislodgment. Previous studies on the bifurcation model mainly investigated the bubble splitting and to which daughter tubes the bubble would travel.[3,19,20,22] A treelike structure, which is the most complicated network reported in the literature, has been intensively investigated for mixing efficiency, pressure drop, mass and heat-transfer rate in the applications of electronic cooling,[23] fuel cells,[24] and chemical reactors.[25−28] However, most of the treelike structures manufactured or simulated in the literature studies are symmetrical dichotomous, which have straight channels and junctions without smooth change.

In this study, the capillary network is designed with a smooth flow path to closely mimic the structure of the physiological vascular networks.[29] The designed network is featured by multichannels and multibifurcations. The distribution of the branching channel size nearly obeys Murray's law, which is the basic principle for designing transfer networks. This paper investigates the effect of channel complexity, diverging/converging angles, channel dimensions, and bubble length on the bubble flow resistance and bubble dislodging pressure in the capillary network. A theoretical model has been established to illustrate the underlying physics of bubble dislodgment in a capillary network and to specify the relationship between the bubble length and dislodging pressure. The effects of surface tension, viscosity, surface roughness, contact angle, and thin-film deposition have been considered in the model.

THEORY

Bubble dislodgment from a microchannel is governed by the forces acting upon the bubble. The dominant forces involved are buoyancy force, drag force, viscous force, and surface tension acting around the bubble contact line. Drag force is exerted by the pressure difference between two ends of the bubble and the corner flow on the bubble in the rectangular channel.[30] The buoyancy force is constant as the bubble volume is fixed (the gas is taken as incompressible under the experimental condition). The inertial effect of the bubble is neglected because of the low We number (less than 1).[16,20,31] Capillary number $\left(Ca = \frac{\mu u}{\gamma}\right)$ in this work is approximately in an order of 10^{-4}, which is similar to the capillary number in the human circulatory system (smaller than 10^{-3} for microvessels less than 500 μm).[32] Surface tension around the bubble acts as the "adhesion force" to "glue" the bubble onto the surface of the channel.[13,33] The dislodgment of a bubble from a microchannel occurs when the pressure difference across the bubble is sufficient to against the resistant pressure drop, which is the sum of the capillary pressure drop and frictional pressure drop.

Capillary Pressure Drop. The capillary pressure difference across the bubble can be reasonably expressed as the function of surface tension and curvatures of the menisci based on the Young−Laplace equation as reported in many literature studies.[34−37] At the initial movement of the bubble, the curvature of menisci can be taken as the function of the cross-sectional area of the microchannel and the advancing and receding contact angle. For a rectangular microchannel, the capillary pressure drop ΔP_c could be expressed by eq 1[16,38]

$$\Delta P_c = 2\sigma\left(\frac{1}{W_j} + \frac{1}{H_j}\right)(\cos\theta_{rec} - \cos\theta_{adv}) \quad (1)$$

where σ is the surface tension, W and H are the channel width and height, respectively, and subscript j represents the corresponding microchannel.

Frictional Pressure Drop. According to the lubrication theory, a liquid film exists between the bubble and the channel wall when an elongated bubble moves in a straight channel filled with liquid. This liquid film is uniform between two bubble ends, and it is of order $Ca^{2/3}$ in thickness.[30,39] Because of the negligible of gravitational force and shear force of the gas

DOI: 10.1021/acs.langmuir.8b03323
Langmuir 2019, 35, 3194−3203

phase, the liquid film is commonly assumed to be stagnant. The frictional resistance to bubble motion arises from liquid films,[40] and the frictional pressure drop for the bubble−liquid flow through a channel with a diameter of D can be calculated through the Darcy−Weisbach equation[8,35,41]

$$\Delta P_f = 2\rho f_f u^2 \frac{\Delta L}{D} \quad (2)$$

where u is the mean superficial velocity and f_f is the frictional factor. In laminar flow (Re number is less than 10 in this study), f_f can be estimated through $f_f = \frac{16}{Re_m}$, where Re_m is the Reynolds number of the mixture, given as

$$Re_m = \frac{\rho u D}{\mu_m} \quad (3)$$

where μ_m is the mixture viscosity, which can be evaluated through many correlations.[42−44]

MATERIALS AND METHOD

Experimental Setups. The structure of a capillary network is designed (Figure 1b) based on Murray's law, which states that under ideal conditions, when a parent blood vessel branches into daughter vessels, the cube of the radius of the parent vessel is equal to the sum of the cubes of the radii of daughter blood vessels.[29] The capillary network used in this study was engraved on an acrylic sheet (2 mm, Acrylic Cast, AMARI, the contact angle is around 68°[45]) with a fusion laser engraving and cutting system (Epilog laser fusion M2). As the leaser cutting cannot make a circular cross section, the shape of the channel cross sections was rectangular in this study. In practice, for example, in electronic devices, electrodes, and porous rocks, the microchannels are not necessary to have a circular cross section. The blood vessels in human body also have noncircular cross sections according to the anatomic quantifications. The circular shape of blood vessels can distort and change with dilation and constriction.[46] We have considered the effect of the rectangular shape on fluid transport in the Modeling section. In rectangular channels, the liquid either pushes the bubble (plug flow) or bypasses the bubble through the corner channels (corner flow). Within the flow rate range used in this study, the flow in polygonal channels obeys the nonlinear pressure−velocity relation, as flows in circular channels.[30,32,47] The channel height (H), width (W), and length (L) were all measured by the microscope, as shown in Table 1.

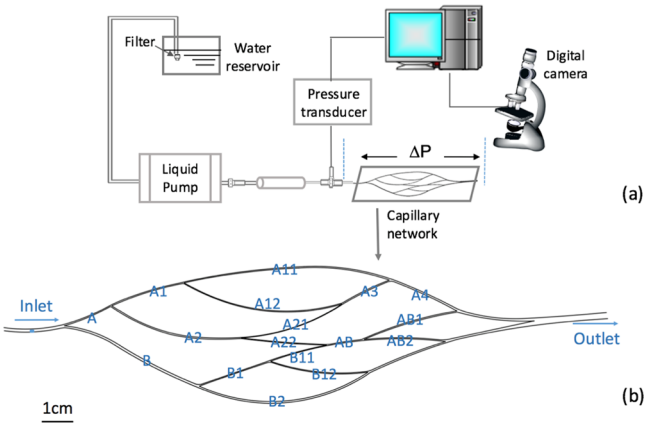

Figure 1. (a) Schematic of the experimental setup: ΔP is the pressure difference between the inlet and outlet of the capillary network and (b) schematic diagram of the designed capillary network (each channel in the capillary network is labeled).

Table 1. Parameters of Microchannels in the Capillary Network (the Channel Height for Microchannels Listed below Is Uniform, Approximately 0.32 mm)

channel	width (mm)	length (cm)	channel	width (mm)	length (cm)
A11	0.46	6.15	AB1	0.45	2.65
A12	0.46	5.05	AB2	0.45	2.4
A2	0.52	4.55	B1	0.40	2.2
A21	0.26	2.95	B11	0.36	1.55
A22	0.37	2.4	B12	0.41	3.0

A liquid delivery pump with a resolution of 0.0001 mL/min (LC-20 AD, Shimadzu) is used to adjust the driving pressure for fluid flows and to control the liquid volumetric flow rate. A digital pressure transducer (DPI 280, Druck) with a resolution of 0.01 mbar is employed to measure the overall pressure drop for fluid flows in the capillary network. The image of bubble motion is recorded through a long working distance microscope (Brunel Microscope Ltd, 10× objective) fitted with a digital camera (AM7023 Dino-Eye, Dino-Lite Digital Microscope).

Measurement of Bubble Dislodging Pressure in the Capillary Network. In this study, the capillary network was maintained in a horizontal configuration. A bubble was injected into the capillary network, which was initially filled with deionized (DI) water. The liquid pump was then operated at a flow rate of 0.1 mL/min. At the beginning, the driving pressure across the bubble was low and only for slowly delivering the bubble into the first bifurcation. Once the bubble was stuck in somewhere of a channel, the driving pressure was increased slowly to a point at which the bubble was dislodged from the capillary network. At the moment when the bubble was dislodged, the pressure measured over the capillary network was accounted as the dislodging pressure (ΔP). The pressure was recorded at the inlet of the capillary network through the pressure transducer. To eliminate the impact of other bubbles on the measured dislodging pressure, only one bubble was in the network channel for every individual measurement. The pressure drop caused by liquid flows (DI water only) in the capillary network was also measured as the reference data. Images of bubble were taken through the video-fitted microscope to measure the bubble length (from the leading tip to the trailing edge of the bubble) and contact angle. As the measurement is easily affected by some noise or fluctuations of the operations, more than 600 bubbles were measured and analyzed to ensure the data reliable. The measurement error of dislodging pressure for the bubbles is below 10%.

RESULTS AND DISCUSSION

When a bubble flows in a capillary network, it may lodge at some points of the microchannels because of the sudden change in channel size or angle, surface roughness, fluid interactions, etc. Dislodgment of the trapped bubbles has been investigated in simple microchannels or networks, such as straight microchannels or microvessels[13,15,16,45,48] and the Y-type channels.[14,22,49] In this paper, experiments were designed to quantitatively investigate the factors affecting the dislodging pressure and bubble dislodgment behavior in a capillary network with asymmetric bifurcations, particularly the effect of bubble length, network structure, and channel dimension on the dislodging pressure.

Effect of Bubble Length on the Dislodging Pressure. The dislodging pressure for bubbles with different lengths in the same channel of the capillary network is plotted in Figure 2 and 3. The graphs clearly demonstrate that there is a critical bubble length (about 2 mm in this study). When the bubble length is less than the critical length, the dislodging pressure for smaller bubbles is greater than that for bubbles with a larger length in the same channel, and the dislodging pressure

DOI: 10.1021/acs.langmuir.8b03323
Langmuir 2019, 35, 3194−3203

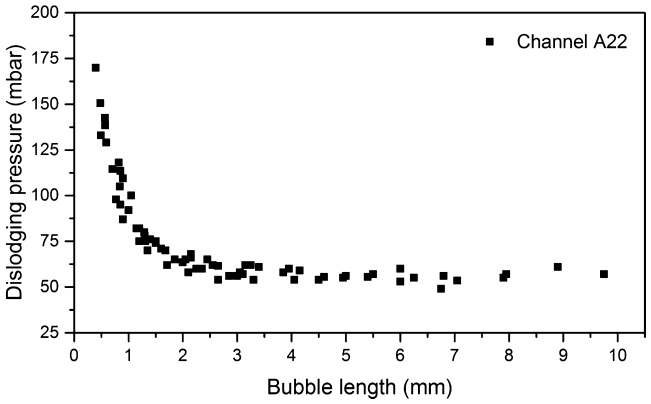

Figure 2. Dislodging pressure for bubbles with different lengths in channel A22.

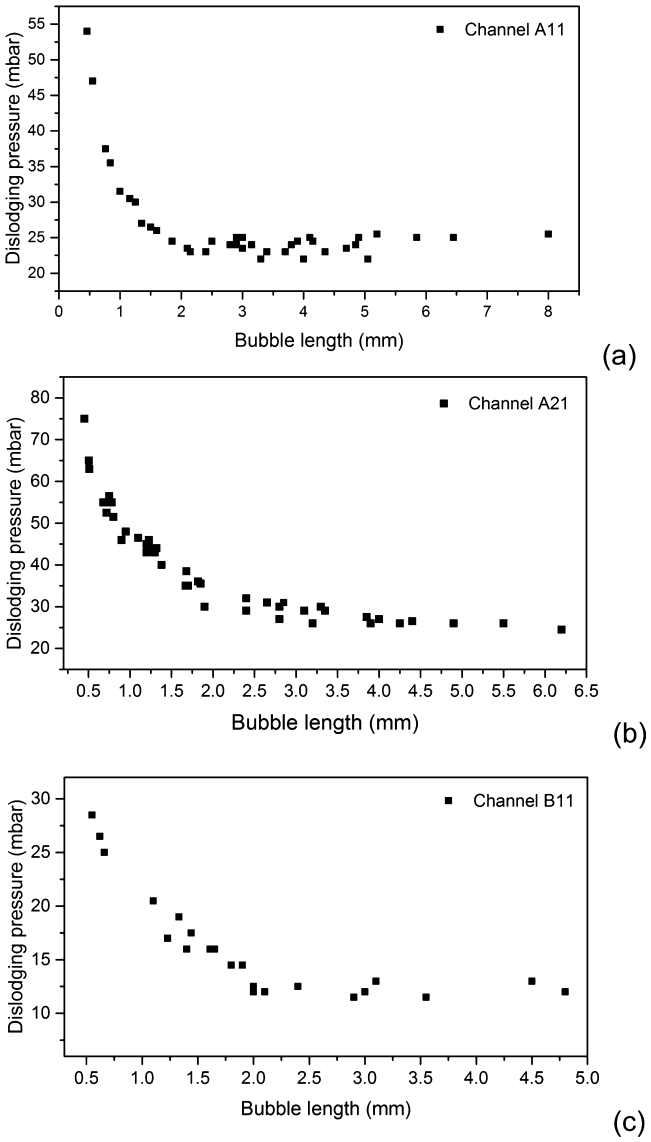

Figure 3. Dislodging pressure for bubbles with different lengths in channels (a) A11, (b) A21, and (c) B11.

increases with the decrease of bubble length. Once the bubble length is greater than 2 mm, the dislodging pressure is almost constant and independent of the bubble length.

Figure 2 shows bubble dislodging pressure profile in channel A22. The same trend has been observed in all other channels of the capillary network, but the magnitude of dislodging pressure varies significantly with channels. For example, in Figures 2 and 3, the dislodging pressure for a bubble with a length of 1 mm is about 92 mbar in channel A22, 32 mbar in channel A11, 47.5 mbar in channel A21, and 20 mbar in channel B11. The significant difference in the dislodging pressure is caused by not only the channel dimension but also the network structure. This will be discussed in the next section.

To the authors' best knowledge, this relationship between the dislodging pressure and bubble length in a complex capillary network has not been reported yet. Very few studies have been conducted to measure the dislodging pressure for bubbles with a length in a large range in a microscopic capillary network. Blackmore et al. and Cavanagh et al. reported that smaller bubbles require a higher dislodging pressure in a straight channel.[15,45] Both two groups did not illustrate the explicit relationship between the dislodging pressure and bubble length. Cavanagh et al. demonstrated that a higher liquid flow rate is required to dislodge smaller bubbles as smaller bubbles have less contact force because of the smaller surface area. They simply lumped all forces acting on the bubble as the contact force, which is too vague to represent the complicated forces involved in bubble dislodgment.

Effect of the Network Structure and Channel Size on the Bubble Dislodging Pressure. The diverging/converging angles of bifurcations, channel dimension, and the complexity of the flow path affect the bubble dislodging pressure through affecting energy loss and fluid velocity. In this study, as $1 < Re < 10$, the inertia of the liquid cannot be neglected compared with the viscous effect.[50−52] When the liquid flows through a channel with curvature, the liquid inertia will contribute to the velocity mismatch in the downstream direction between the liquid in the central and near-wall regions. The velocity mismatch causes the energy dissipation, and thus, the liquid velocity will be smaller in the channel with curvature than the velocity in the straight channel under the same injection flow rate. As the driving force is proportional to the liquid velocity, the driving force to dislodge the bubble is smaller in a curved channel. For a bubble with the same volume, the dislodging pressure provided at the network inlet will be higher in order to dislodge a bubble in a curved channel than in a straight channel.

Network Structure. The effect of the network structure on the bubble dislodging pressure is discussed in terms of diverging/converging angles and complexity of flow path. The diverging angle of bifurcations is defined as the angle between the diverging fluid and the parent fluid velocity vector as illustrated in Figures 4b, 5b, and 7b. The converging angle is defined in a similar way and shown in Figure 4d.

Figures 4−7 compare the dislodging pressure among different channels and demonstrate how the impact of bubble length on the dislodging pressure varies with the network structure. From the dislodging pressure profiles for channels with similar size and flow condition, we found that the larger the diverging angle and/or converging angle, the higher the pressure is required to dislodge a bubble with the same length.

For example, the dislodging pressure for bubbles in channel A12 is significantly higher than that in channel A11 as shown in Figure 4a. Considering that channels A11 and A12 have similar size ($W \approx 0.46$ mm, $H \approx 0.32$ mm) and they share the

DOI: 10.1021/acs.langmuir.8b03323
Langmuir 2019, 35, 3194−3203

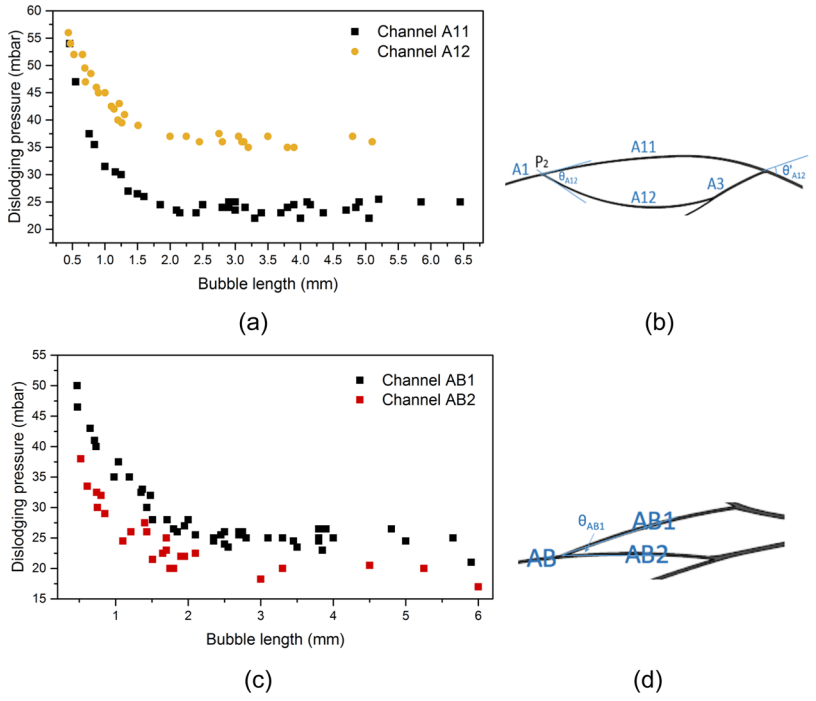

Figure 4. (a) Dislodging pressure profiles for bubbles in channels A11 (W = 0.46 mm) and A12 (W = 0.46 mm); (b) schematic diagram of channels A11 and A12; (c) dislodging pressure profiles for bubbles in channels AB1 and AB2; and (d) schematic diagram of channels AB1 and AB2. (θ_{A12} is the diverging angle of channel A12, θ'_{A12} is the converging angle of channel A12, and θ_{AB1} is the diverging angle of channel AB1).

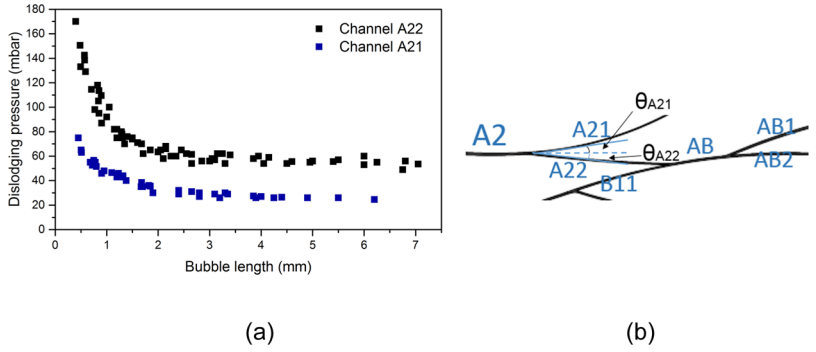

Figure 5. (a) Dislodging pressure profiles for bubbles in channels A21 and A22 and (b) schematic diagram of the network structure around channels A21 and A22 (θ_{A21} and θ_{A22} are the diverging angles of channels A21 and A22, respectively).

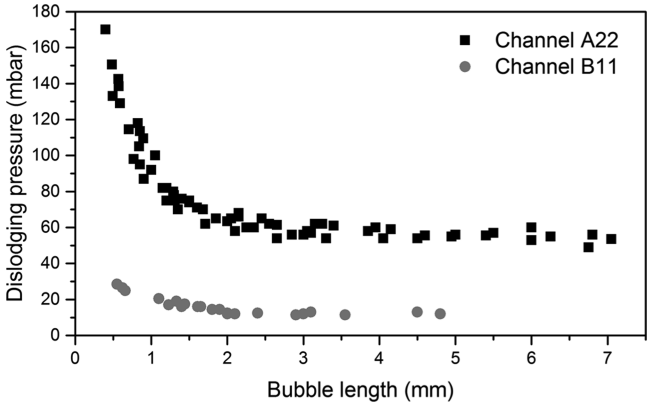

Figure 6. Dislodging pressure profiles for bubbles in channels B11 (W = 0.36 mm) and A22 (W = 0.37 mm).

same inlet (A1) and outlet (A4), the main difference between two channels is the diverging angle ($\theta_{A12} \approx 40.8°$ and $\theta_{A11} \approx 0°$) and converging angle ($\theta'_{A12} \approx 48°$ and $\theta'_{A11} \approx 0°$). Similarly, channels AB1 and AB2 have similar size ($W \approx 0.45$ mm, $H \approx 0.32$ mm), and they share the same inlet (channel AB), as shown in Figure 4d. The dislodging pressure in channel AB1 is greater than that in channel AB2, and the diverging angle of channel AB1 ($\theta_{AB1} \approx 14.4°$, $\theta_{AB2} \approx 0°$) is slightly larger. The comparison of channels A11 and A12 and channels AB1 and AB2 indicates that the diverging and converging angles may have an effect on the bubble dislodging pressure in the network.

To demonstrate the angle effect, we employed the electric circuit analogy to predict the pressure drop across the single channel where the bubble lodges. The circuit method is based on the analogous behavior of hydraulic electric circuits, with correlations of pressure to voltage, volumetric flow rate to current, and hydraulic resistance to electric resistance. The hydraulic resistance (R_H) for the rectangular microchannel can be predicted theoretically according to eq 4.[53,54] As the capillary effect dominates the flow of the blocked channel (Ca

DOI: 10.1021/acs.langmuir.8b03323
Langmuir 2019, 35, 3194−3203

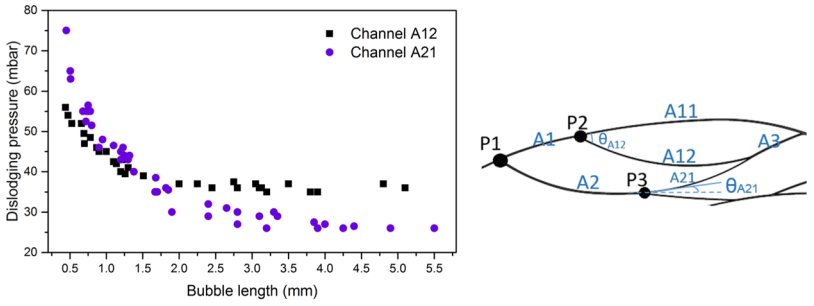

(a) (b)

Figure 7. (a) Dislodging pressure for bubbles with different lengths in channels A12 (W = 0.46 mm) and A21 (W = 0.26 mm) and (b) schematic diagram of the network structure around channels A12 and A21 and θ_{A21} is the diverging angle of channel A21.

$\approx 10^{-4}$), the resistance of the blocked channel is significantly higher than the resistance of other channels. The channel in which the bubble lodges/blocks can be analogized to a resistor with infinite electric resistance. The equivalent electric circuit and equivalent resistors are shown in Figure S1. The pressure across the blocked channel then can be predicted through Simulink, Matlab. For example, the pressure difference between the two ends of channel A11 (ΔP_{A11}) can be calculated through eq 5

$$R_H = \frac{12\sigma L}{wh^3\left\{1 - \frac{h}{w}\left[\frac{192}{\pi^5}\sum_{n=1,3,5}^{\infty}\frac{1}{n^5}\tanh\left(\frac{n\pi w}{2h}\right)\right]\right\}} \quad (4)$$

$$\Delta P_{A11} = \Delta P_{total} - Q_A R_{H(A)} - Q_{A1} R_{H(A1)} - Q_{A4} R_{H(A4)} - Q_{A5} R_{H(A5)} \quad (5)$$

where w, h, and L are the microchannel width, height, and length, respectively, and ΔP_{total} is the experimental overall pressure required to dislodge one bubble from channel A11.

Similarly, the pressure difference between the two ends of channels A12, AB1, and AB2 when dislodging one bubble from the corresponding channel can be obtained following the same procedure. The data are shown in Table S1, which indicates that $\Delta P_{A12} > \Delta P_{A11}$ and $\Delta P_{AB1} > \Delta P_{AB2}$ when the bubble lengths in these channels are the same. The main difference between two sets of channels is the diverging angle ($\theta_{A12} \approx 40.8° > \theta_{A11} \approx 0°$ and $\theta_{AB1} \approx 14.4° > \theta_{AB2} \approx 0°$) and converging angle ($\theta'_{A12} \approx 48° > \theta'_{A11} \approx 0°$). Therefore, the comparison of pressure across the single channels of A11 and A12 and channels of AB1 and AB2 demonstrated that the diverging angle and converging angle affect the dislodging pressure in a complex network.

Another factor affecting the bubble dislodging pressure is the complexity of flow path. It is easy to understand that the fluid is prone to choose the relatively easier way to travel under the same flow rate, as more energy would be lost to travel through a complex flow path. For example, channel A22 (W = 0.37 mm) and channel A21 (W = 0.26 mm) have the same inlet (channel A2), and the diverging angle is similar ($\theta_{A21} \approx \theta_{A22} \approx 7.8°$), while the dislodging pressure in channel A22 is larger than that in channel A21 as shown in Figure 5a. This is mainly attributed to the network complexity, that is, the existence of the channels AB, AB1, and AB2.

Channel Size. In a single capillary, the narrower channel will give a higher resistance to the bubble movement based on the reciprocal relationship between the channel diameter and pressure drop. However, this may not occur in a complex capillary network with high interconnectivity, and the comprehensive effect induced by the complex structure and multichannel features is required to be taken into account when analyzing the bubble dislodgment.

The effect of channel size in this capillary network is not obvious because of the effect of the network structure. For example, channels A22 and B11 have a width of about 0.36 mm, but the bubble dislodging pressure in channel A22 is significantly higher than that in channel B11 as shown in Figure 6. Similar phenomenon has been discussed above in channels A11−A12 and channels AB1−AB2 (Figure 4).

The interplay between the impact of the network structure and the impact of the channel size on the dislodging pressure varies with the bubble length. Taking channels A21 (W = 0.26 mm) and A12 (W = 0.46 mm) as an example, they have the same converged channel (A3) but different inlet channels. Theoretically, the narrower channel (channel A21) should provide a higher resistance to bubble movement. However, as shown in Figure 7a, when the bubble length is larger than around 1.5 mm, the dislodging pressure in channel A12 (wider) is higher than that in channel A21 (narrower). It seems that for large bubbles, the dislodging pressure is dominated by the network structure rather than the channel width. The fluid loses more energy from P1 (as shown in Figure 7b) to reach channel A12 because of the high diverging angle in P2 ($\theta_{A12} \approx 40.8°$) and loses less energy to reach channel A21 because of the lower diverging angle ($\theta_{A21} = 7.8°$) at P3.

For bubbles with a length less than 1.5 mm, the dislodging pressure for bubbles with a similar length in channel A21 (narrower) is higher than that in channel A12 (wider), which is opposite to the dislodging pressure profile for bubbles with a length greater than 1.5 mm. The pressure increase rate in channel A21 is larger than that in channel A12. For example, when the bubble length decreases from 3.1 to 0.5 mm, the dislodging pressure increases from 37.5 to 55 mbar in channel A12 and from 28.5 to 75 mbar in channel A21. This indicates that the channel width influences significantly the dislodging pressure increase rate when the bubble length is less than 1.5 mm. Narrower channels will be more sensitive to the change of bubble length. Further explanation of these phenomena based on our proposed model has been detailed in the next section.

Modeling. The bubble dislodgment in a capillary network is complicated. It involves the effects of bubble length, channel size, network structure, interfacial tension between liquid and gas, the wettability of network material, etc. To consider the influence of the network structure, that is, multichannel, multibifurcation, and bifurcating angles, a parameter c_j is

DOI: 10.1021/acs.langmuir.8b03323
Langmuir 2019, 35, 3194−3203

proposed to represent the contribution of the dislodging pressure from the individual channel j in the network.

Full Model. A theoretical model is proposed to describe the behavior of bubble dislodgment from a microchannel in a complex capillary network. Considering the moment when the motion of the bubble is initiated, a bubble slug as shown in Figure 8 is selected for the following discussion.

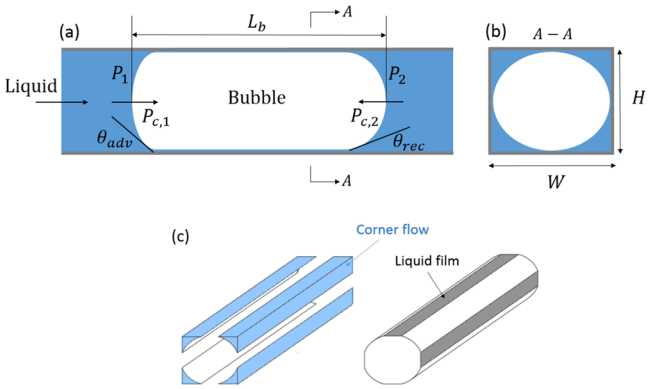

Figure 8. (a) Schematic diagram of a bubble slug in a microchannel of the capillary network in its static state, (b) cross-sectional view of the gas/liquid distribution across the channel, and (c) schematic diagram of the bubble flow through a microchannel in which liquid flows past the bubble through the corner.

We assume that the pressure drop through the bubble slug is equal to the pressure difference between the pressure in bubble left end (P_1) and pressure in bubble right end (P_2), that is,

$$\Delta P_{\text{bubble}} = P_1 - P_2 \tag{6}$$

By applying a driving pressure to the bubble, the shape of the bubble will be deformed against the bubble movement; thus, a capillary pressure drop is induced because of the difference between the left and right curvatures.[16,38] The frictional force exists between the liquid film and the bubble phase, acting as another resistant force for the bubble movement.[40] The resistant pressure drop for the bubble movement (ΔP_{bubble}) is thus the sum of the frictional pressure drop (ΔP_{f}) and the capillary pressure drop (ΔP_{c}), that is,

$$\Delta P_{\text{bubble}} = \Delta P_{\text{f}} + \Delta P_{\text{c}} \tag{7}$$

The capillary pressure drop is calculated by eq 1. The frictional pressure drop caused by the liquid film can be calculated based on the Darcy–Weisbach equation, which shows a good prediction in several previous studies.[35,55−57] In the bubble slug unit, the frictional pressure drop ΔP_{f} can be written based on eq 2[8,35,41] as

$$\Delta P_{\text{f}} = 2\rho_{\text{l}} f_{\text{f}} u_{\text{b}}^{\,2} \frac{l_{\text{b}}}{H_j} \tag{8}$$

where ρ_{l} is the density of DI water, u_{b} is the mean superficial velocity of the bubble, l_{b} is the length of the bubble slug (bubble length), and H_j is the height of the corresponding microchannel.

The driving pressure around the bubble is maintained by the corner flow, as the corner liquid (the blue section, as depicted in Figure 8b,c) drags the bubble to move. The pressure drop for the corner flow is equal to the driving pressure exerting on the bubble, which was also assumed by Wong et al. and Mohammadi.[16,38] As the liquid flowing across the corner can be treated as Poiseuille flow, the pressure drop for the corner flow can be approximately calculated based on the Poiseuille law, given as

$$P_1 - P_2 = \frac{128\mu_{\text{l}} l_{\text{b}} Q_{\text{f}}}{\pi D_{\text{eff}}^{\,4}} \tag{9}$$

where μ_{l} is the viscosity of DI water, Q_f is the volumetric flow rate, and D_{eff} is the effective dynamic diameter of the liquid flow in corners, which can be assumed as a constant for each microchannel in this study.

In this capillary network, the volumetric flow rate Q_{f} is the function of the pressure difference between the inlet and outlet of the microchannel (ΔP_j) and can be expressed according to Darcy's law[58]

$$Q_{\text{f}} = -\frac{KK_{\text{r,f}}A}{\mu_{\text{l}}}\frac{\partial p}{\partial x} = \frac{KK_{\text{r,f}}A_j}{\mu_{\text{l}}}\frac{\Delta P_j}{L_j} \tag{10}$$

$$\Delta P_j = c_j \times \Delta P$$

where K is the absolute permeability of the microchannel, $K_{\text{r,f}}$ is the relative permeability of fluid, A is the sectional area of the microchannel, L is the length of the microchannel, ΔP_j is the pressure drop in microchannel j, and ΔP is the overall pressure difference between the inlet and outlet of the capillary network.

Parameter c_j, a pressure loss factor of the corresponding microchannel j, is defined to characterize the pressure loss caused by network structures (such as multichannel, multi-bifurcation, and bifurcating angles), given as $c_j = \frac{\Delta P_j}{\Delta P}$. It can be seen as the contribution of the dislodging pressure in the individual channel j in the network.

Combining 6, the pressure difference initiating the bubble movement can be expressed as

$$\Delta P = \frac{\pi D_{\text{eff}}^{\,4} L_j}{64KK_{\text{r,f}}W_j H_j c_j}\left[\frac{\sigma\left(\frac{1}{W_j}+\frac{1}{H_j}\right)(\cos\theta_{\text{rec}} - \cos\theta_{\text{adv}})}{l_{\text{b}}} + \frac{\rho_{\text{l}} f_{\text{f}} u_{\text{b}}^{\,2}}{H_j}\right] \tag{11}$$

The relative permeability $K_{\text{r,f}}$ is related to the void fraction (the fraction of the channel cross-sectional area that is occupied by the bubble, as shown in Figure 8b), and it can be approximately taken as an invariable. The difference in the cosine of the receding and advancing angle changes in a small range, which can be roughly neglected.

Equation 11 can be written as a simple form

$$\Delta P = \frac{\text{MA}_j}{l_{\text{b}}} + \text{NB}_j \tag{12}$$

in which

$$A_j = \frac{L_j}{W_j H_j c_j}\left(\frac{1}{W_j}+\frac{1}{H_j}\right), \qquad B_j = \frac{L_j}{W_j H_j^{\,2} c_j} \tag{13}$$

$$M = \frac{\sigma\pi D_{\text{eff}}^{\,4}}{64KK_{\text{r,f}}}(\cos\theta_{\text{rec}} - \cos\theta_{\text{adv}}), \qquad N = \frac{\pi D_{\text{eff}}^{\,4}\rho_{\text{l}} f_{\text{f}} u_{\text{b}}^{\,2}}{64KK_{\text{r,f}}} \tag{14}$$

where A_j and B_j are the parameters related to the corresponding microchannel and M and N are constant for the same microchannel.

DOI: 10.1021/acs.langmuir.8b03323
Langmuir 2019, 35, 3194−3203

Analysis of Experimental Results. The model proposed in eq 11 fully describes the factors affecting the dislodging pressure for a single bubble in a capillary network with multichannel and multibifurcation. It closely relates to the channel dimension (width, length, and height), bubble length, fluid flow rate, contact angle, and network structure. The impact of the network structure and channel size on the dislodging pressure has been discussed quantitatively. In this section, experimental results will be analyzed through combining the model with parameters MA_j and NB_j as well as parameter c_j.

This model demonstrates that the dislodging pressure is dependent on the bubble length (l_b) in a complex capillary network. For bubbles with small lengths, the dislodging pressure increases significantly with the decrease of bubble length, that is, a smaller bubble will require higher pressure to dislodge. When the bubble length is longer than a certain value, the dislodging pressure is nearly equal to a constant (NB_j) and is independent of the bubble length for a fixed channel and flow conditions. This model matches very well with our experimental results, and the dislodging pressure profile for every channel in this network fits eq 12 with a very high *R*-square value, as shown in the Supporting Information (Figure S2).

Equation 12 illustrates that parameter MA_j corresponds to the increase rate of the dislodging pressure, and parameter NB_j is the dislodging pressure of bubbles with infinite length (the nearly horizontal section of the pressure profile). The ratio of parameters MA_j and NB_j for each channel can be obtained from the experimental dislodging pressure. Figure 9 indicates

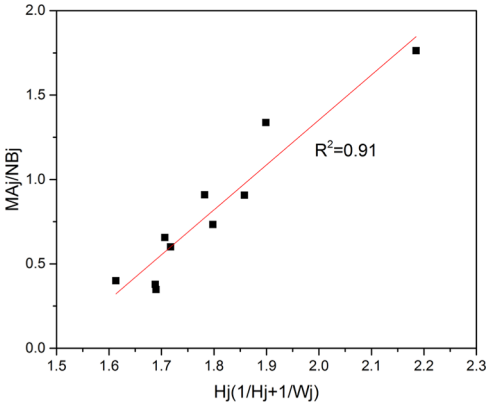

Figure 9. Plot of the parameter ratio of MA_j/NB_j vs the dimensionless constant $H_j\left(\frac{1}{W_j}+\frac{1}{H_j}\right)$; the red line represents the best fit line.

that the ratio of parameters (MA_j/NB_j) varies linearly with $H_j\left(\frac{1}{W_j}+\frac{1}{H_j}\right)$, which is in good agreement with the correlation (13) derived based on eq 12.

$$\frac{MA_j}{NB_j} = CH_j\left(\frac{1}{W_j}+\frac{1}{H_j}\right) \tag{15}$$

in which *C* is a constant for the corresponding channel *j*.

According to eq 11, parameters MA_j and NB_j are both proportional to the channel length (L) and inversely proportional to the channel size (W and H) and parameter c_j. Parameter c_j characterizes the effect of the network structure, that is, multichannels, multibifurcations, and channel complexity, on the dislodging pressure. A small magnitude of parameter c_j indicates that the impact of the network structure on the dislodging pressure is significant. In Figure 10a, channels A12, A22, and B12 have a relatively high parameter NB_j among other channels. These three channels are not characterized by the longest length or smallest channel size. The relatively high value of parameter NB_j is attributed to the smaller value of parameter c_j because of the bifurcating angles. The magnitude of NB_j for channel A11 and channel A21 is not noticeably high even though channel A11 has the longest length and channel A21 has the smallest channel size. This indicates that the impact of channel size and channel length on the parameter NB_j is not obvious. Therefore, parameter c_j rather than the channel dimension dominates the magnitude of NB_j of microchannels in a capillary network. In other words, the network structure rather than the channel dimension dominates the dislodging pressure for bubbles with long length in a complex capillary network.

Although the channel size does not markedly affect the magnitude of NB_j, it takes more effect on the parameter MA_j. As shown in eq 13, parameter MA_j is inversely proportional to W^2 (channel width), whereas parameter NB_j is only affected by W. From Figure 10b, channel A21 has the second largest magnitude of MA_j (around 33 mbar mm), even though the c_j value of channel A21 is large and the length of channel A21 is small (L_{A21} = 2.95 cm). The reason for the large MA_j of channel A21 is the smallest channel width (W_{A21} = 0.26 mm), that is, the channel width affects MA_j significantly.

The analysis of parameters MA_j, NB_j, and c_j has clearly explained the experimental data and the effect of bubble length and network structure on the dislodging pressure in previous sections. For example, for bubbles with a large length, the dislodging pressure for bubbles in channel A12 is higher than that in channel A21 (as shown in Figure 7a) because of the dominant impact of the network structure. This explanation agrees well with the analysis of parameter NB_j (corresponding to the dislodging pressure for long bubbles), which is dominated by the parameter c_j. For bubbles with small length, the dislodging pressure in channel A21 becomes higher than that in channel A12 owing to the effect of channel width. This is in line with the analysis of parameter MA_j as the dislodging pressure of small bubbles is significantly affected by the increase rate (i.e., parameter MA_j), which highly depends on the channel width.

CONCLUSIONS

The bubble dislodgment in a complex capillary network has been investigated in terms of the bubble length, diverging/converging angle, channel complexity, and channel dimensions (length, height, and width). The dislodging pressure profiles demonstrate that there is a critical bubble length for every microchannel of the network. When the bubble length is less than this critical value, the dislodging pressure will increase with the decrease of the bubble length, that is, smaller bubbles require higher dislodging pressure. When the bubble length is longer than the critical value, the dislodging pressure is independent of the bubble length. Every channel of the capillary network has a similar trend of dislodging pressure−bubble length profile. Furthermore, the effect of the diverging/converging angle and channel size has been investigated through comparing the dislodging pressure profiles among different channels. Generally, higher dislodging pressure is

DOI: 10.1021/acs.langmuir.8b03323
Langmuir 2019, 35, 3194−3203

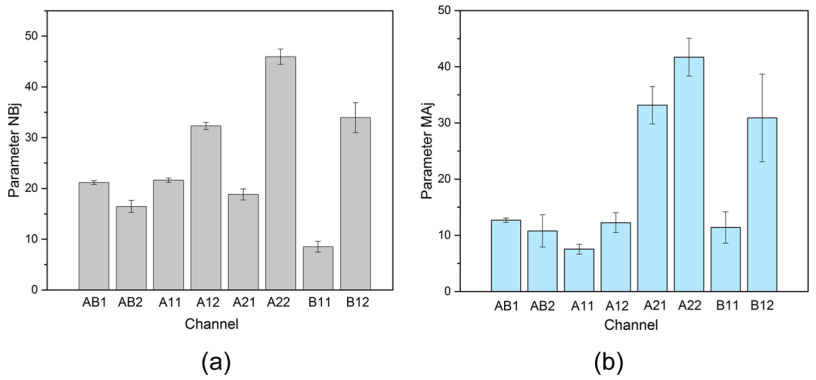

Figure 10. Comparison of (a) parameter NB_j and (b) MA_j among different channels in the capillary network.

required for bubbles with the same length in the channel with diverging/converging angles.

A one-dimensional model has been derived to fully describe the bubble dislodgment in a complex capillary network and to predict the dislodging pressure. Parameter c_j is introduced to characterize the effect of the network structure (i.e., multichannel and multibifurcation features) on the dislodging pressure. The model agrees well with the experimental results. In this capillary network, parameter NB_j is dominated by parameter c_j (network structure effect) and the increase rate of the dislodging pressure (parameter MA_j) is affected significantly by both the channel width and parameter c_j. This model has been validated and could be employed in other capillary networks.

■ ASSOCIATED CONTENT

Supporting Information

The Supporting Information is available free of charge on the ACS Publications website at DOI: 10.1021/acs.langmuir.8b03323.

Schematic of the equivalent fluidic circuit and fluidic resistors; pressure difference across single channels; and diagrams of dislodging pressure profiles for bubbles in each channel of the complex capillary network (PDF)

■ AUTHOR INFORMATION

Corresponding Author

*E-mail: x.fan@ed.ac.uk.

ORCID

Cong Chao: 0000-0001-6738-5732

Xianfeng Fan: 0000-0002-6811-953X

Notes

The authors declare no competing financial interest.

■ REFERENCES

(1) Farajzadeh, R.; Andrianov, A.; Krastev, R.; Hirasaki, G. J.; Rossen, W. R. Foam-oil interaction in porous media: Implications for foam assisted enhanced oil recovery. *Adv. Colloid Interface Sci.* **2012**, *183*−*184*, 1−13.

(2) Bull, J. L. Cardiovascular bubble dynamics. *Crit. Rev. Biomed. Eng.* **2005**, *33*, 299−346.

(3) Valassis, D. T.; Dodde, R. E.; Esphuniyani, B.; Fowlkes, J. B.; Bull, J. L. Microbubble transport through a bifurcating vessel network with pulsatile flow. *Biomed. Microdevices* **2011**, *14*, 131−143.

(4) Yang, H.; Zhao, T. S.; Ye, Q. In situ visualization study of CO2 gas bubble behavior in DMFC anode flow fields. *J. Power Sources* **2005**, *139*, 79−90.

(5) Calabriso, A.; Borello, D.; Romano, G. P.; Cedola, L.; Del Zotto, L.; Santori, S. G. Bubbly flow mapping in the anode channel of a direct methanol fuel cell via PIV investigation. *Appl. Energy* **2017**, *185*, 1245−1255.

(6) Steinbrenner, J. E.; Lee, E. S.; Hidrovo, C. H.; Eaton, J. K.; Goodson, K. E. Impact of channel geometry on two-phase flow in fuel cell microchannels. *J. Power Sources* **2011**, *196*, 5012−5020.

(7) Chen, X.; Zhang, Z.; Yi, D.; Hu, Z. Numerical studies on different two-dimensional micromixers basing on a fractal-like tree network. *Microsyst. Technol.* **2015**, *23*, 755−763.

(8) Yue, J.; Chen, G.; Yuan, Q. Pressure drops of single and two-phase flows through T-type microchannel mixers. *Chem. Eng. J.* **2004**, *102*, 11−24.

(9) Boehm, T.; Folkman, J.; Browder, T.; O'Reilly, M. S. Antiangiogenic therapy of experimental cancer does not induce acquired drug resistance. *Nature* **1997**, *390*, 404.

(10) Bull, J. L. The application of microbubbles for targeted drug delivery. *Expert Opin. Drug Delivery* **2007**, *4*, 475−493.

(11) Samuel, S.; Duprey, A.; Fabiilli, M. L.; Bull, J. L.; Brian Fowlkes, J. In vivo microscopy of targeted vessel occlusion employing acoustic droplet vaporization. *Microcirculation* **2012**, *19*, 501−509.

(12) Hernot, S.; Klibanov, A. L. Microbubbles in ultrasound-triggered drug and gene delivery. *Adv. Drug Delivery Rev.* **2008**, *60*, 1153−1166.

(13) Suzuki, A.; Eckmann, D. M. Embolism bubble adhesion force in excised perfused microvessels. *Anesthesiology* **2003**, *99*, 400−408.

(14) Calderón, A. J.; Heo, Y. S.; Huh, D.; Futai, N.; Takayama, S.; Fowlkes, J. B.; Bull, J. L. Microfluidic model of bubble lodging in microvessel bifurcations. *Appl. Phys. Lett.* **2006**, *89*, 244103.

(15) Blackmore, B.; Li, D.; Gao, J. Detachment of bubbles in slit microchannels by shearing flow. *J. Colloid Interface Sci.* **2001**, *241*, 514−520.

(16) Mohammadi, M.; Sharp, K. V. The Role of Contact Line (Pinning) Forces on Bubble Blockage in Microchannels. *J. Fluids Eng.* **2015**, *137*, 0312081−312087.

(17) Banerjee, S.; Hassenklöver, E.; Kleijn, J. M.; Cohen Stuart, M. A.; Leermakers, F. A. M. Interfacial tension and wettability in water-carbon dioxide systems: experiments and self-consistent field modeling. *J. Phys. Chem. B* **2013**, *117*, 8524−8535.

(18) Schäffer, E.; Wong, P.-z. Contact line dynamics near the pinning threshold: A capillary rise and fall experiment. *Phys. Rev. E: Stat. Phys., Plasmas, Fluids, Relat. Interdiscip. Top.* **2000**, *61*, 5257.

(19) Calderon, A. J.; Eshpuniyani, B.; Fowlkes, J. B.; Bull, J. L. A boundary element model of the transport of a semi-infinite bubble through a microvessel bifurcation. *Phys. Fluids* **2010**, *22*, 061902.

(20) Calderón, A. J.; Fowlkes, J. B.; Bull, J. L. Bubble splitting in bifurcating tubes: a model study of cardiovascular gas emboli transport. *J. Appl. Physiol.* **2005**, *99*, 479−487.

(21) Carlson, A.; Do-Quang, M.; Amberg, G. Droplet dynamics in a bifurcating channel. *Int. J. Multiphase Flow* **2010**, *36*, 397−405.

DOI: 10.1021/acs.langmuir.8b03323
Langmuir 2019, 35, 3194−3203

(22) Eshpuniyani, B.; Fowlkes, J. B.; Bull, J. L. A bench top experimental model of bubble transport in multiple arteriole bifurcations. *Int. J. Heat Fluid Flow* **2005**, *26*, 865−872.
(23) Escher, W.; Michel, B.; Poulikakos, D. Efficiency of optimized bifurcating tree-like and parallel microchannel networks in the cooling of electronics. *Int. J. Heat Mass Transfer* **2009**, *52*, 1421−1430.
(24) Senn, S. M.; Poulikakos, D. Tree network channels as fluid distributors constructing double-staircase polymer electrolyte fuel cells. *J. Appl. Phys.* **2004**, *96*, 842−852.
(25) Chen, Y.; Zhang, C.; Wu, R.; Shi, M. Methanol steam reforming in microreactor with constructal tree-shaped network. *J. Power Sources* **2011**, *196*, 6366−6373.
(26) Gosselin, L. Optimization of tree-shaped fluid networks with size limitations. *Int. J. Therm. Sci.* **2007**, *46*, 434−443.
(27) Bello-Ochende, T.; Liebenberg, L.; Meyer, J. P. Constructal cooling channels for micro-channel heat sinks. *Int. J. Heat Mass Transfer* **2007**, *50*, 4141−4150.
(28) da Silva, A. K.; Bejan, A. Constructal multi-scale structure for maximal heat transfer density in natural convection. *Int. J. Heat Fluid Flow* **2005**, *26*, 34−44.
(29) Chen, Y.; Deng, Z. Gas flow in micro tree-shaped hierarchical network. *Int. J. Heat Mass Transfer* **2015**, *80*, 163−169.
(30) Wong, H.; Radke, C. J.; Morris, S. The motion of long bubbles in polygonal capillaries. Part 2. Drag, fluid pressure and fluid flow. *J. Fluid Mech.* **2006**, *292*, 95−110.
(31) Kreutzer, M. T.; Kapteijn, F.; Moulijn, J. A.; Kleijn, C. R.; Heiszwolf, J. J. Inertial and interfacial effects on pressure drop of Taylor flow in capillaries. *AIChE J.* **2005**, *51*, 2428−2440.
(32) Bento, D.; Sousa, L.; Yaginuma, T.; Garcia, V.; Lima, R.; Miranda, J. M. Microbubble moving in blood flow in microchannels: effect on the cell-free layer and cell local concentration. *Biomed. Microdevices* **2017**, *19*, 6.
(33) Eckmann, D. M.; Cavanagh, D. P. Bubble detachment by diffusion-controlled surfactant adsorption. *Colloids Surf., A* **2003**, *227*, 21−33.
(34) Dussan V, E. B.; Chow, R. T.-P. On the Ability of Drops or Bubbles to Stick to Non-Horizontal Surfaces of Solids. *J. Fluid Mech.* **1983**, *137*, 1−29.
(35) Younes, A.; Hassan, I.; Kadem, L. Investigation of Bubble Frequency for Slug Flow Regime in a Uniformly Heated Horizontal Microchannel. *J. Heat Trans.-T. ASME* **2017**, *139*, 061501.
(36) Paust, N.; Litterst, C.; Metz, T.; Eck, M.; Ziegler, C.; Zengerle, R.; Koltay, P. Capillary-driven pumping for passive degassing and fuel supply in direct methanol fuel cells. *Microfluid. Nanofluid.* **2009**, *7*, 531−543.
(37) Gaakeer, W. A.; de Croon, M. H. J. M.; van der Schaaf, J.; Schouten, J. C. Liquid-liquid slug flow separation in a slit shaped micro device. *Chem. Eng. J.* **2012**, *207*−*208*, 440−444.
(38) Wong, C. W.; Zhao, T. S.; Ye, Q.; Liu, J. G. Transient capillary blocking in the flow field of a micro-DMFC and its effect on cell performance. *J. Electrochem. Soc.* **2005**, *152*, A1600−A1605.
(39) Bretherton, F. P. The Motion of Long Bubbles in Tubes. *J. Fluid Mech.* **2006**, *10*, 166−188.
(40) Ma, S.; Mason, G.; Morrow, N. R. Effect of contact angle on drainage and imbibition in regular polygonal tubes. *Colloids Surf., A* **1996**, *117*, 273−291.
(41) Kawahara, A.; Chung, P. M.-Y.; Kawaji, M. Investigation of two-phase flow pattern, void fraction and pressure drop in a microchannel. *Int. J. Multiphase Flow* **2002**, *28*, 1411−1435.
(42) McAdams, W. H. *Heat Transmission*. 3rd ed.; McGraw-Hill: New York, 1954.
(43) Cicchitti, A.; Silvestri, M.; Solddaini, G.; Zavalluilli, R. Two-phase cooling experiments−Pressure drop, heat transfer and burnout measurement. *Energ. Nucl.* **1960**, *7*, 407−425.
(44) Dukler, A. E.; Wicks, M.; Cleveland, R. G. Frictional pressure drop in two-phase flow: A. A comparison of existing correlations for pressure loss and holdup. *AIChE J.* **1964**, *10*, 38−43.
(45) Cavanagh, D. P.; Eckmann, D. M. Interfacial dynamics of stationary gas bubbles in flows in inclined tubes. *J. Fluid Mech.* **1999**, *398*, 225−244.
(46) Gao, Y.-R.; Drew, P. J. Determination of vessel cross-sectional area by thresholding in Radon space. *J. Cereb. Blood Flow Metab.* **2014**, *34*, 1180−1187.
(47) Chung, P. M.-Y.; Kawaji, M.; Kawahara, A.; Shibata, Y. Two-Phase Flow through Square and Circular Microchannels: Effect of Channel Geometry. *ASME/JSME 2003 4th Joint Fluids Summer Engineering Conference*; American Society of Mechanical Engineers, 2003; pp 1459−1467.
(48) Fuerstman, M. J.; Lai, A.; Thurlow, M. E.; Shevkoplyas, S. S.; Stone, H. A.; Whitesides, G. M. The pressure drop along rectangular microchannels containing bubbles. *Lab Chip* **2007**, *7*, 1479−1489.
(49) Poornima, J.; Vengadesan, S. Numerical simulation of bubble transport in a bifurcating microchannel: a preliminary study. *J. Biomech. Eng.* **2012**, *134*, 081005.
(50) Debus, J.-D.; Mendoza, M.; Succi, S.; Herrmann, H. J. Energy dissipation in flows through curved spaces. *Sci. Rep.* **2017**, *7*, 42350.
(51) Zhang, J.; Yan, S.; Yuan, D.; Alici, G.; Nguyen, N.-T.; Ebrahimi Warkiani, M.; Li, W. Fundamentals and applications of inertial microfluidics: a review. *Lab Chip* **2016**, *16*, 10−34.
(52) Di Carlo, D. Inertial microfluidics. *Lab Chip* **2009**, *9*, 3038−3046.
(53) Oh, K. W.; Lee, K.; Ahn, B.; Furlani, E. P. Design of pressure-driven microfluidic networks using electric circuit analogy. *Lab Chip* **2012**, *12*, 515−545.
(54) Kim, D.; Chesler, N. C.; Beebe, D. J. A method for dynamic system characterization using hydraulic series resistance. *Lab Chip* **2006**, *6*, 639−644.
(55) Walsh, E.; Muzychka, Y.; Walsh, P.; Egan, V.; Punch, J. Pressure drop in two phase slug/bubble flows in mini scale capillaries. *Int. J. Multiphase Flow* **2009**, *35*, 879−884.
(56) Chung, P. M.-Y.; Kawaji, M. The effect of channel diameter on adiabatic two-phase flow characteristics in microchannels. *Int. J. Multiphase Flow* **2004**, *30*, 735−761.
(57) Kreutzer, M. T.; Kapteijn, F.; Moulijn, J. A.; Heiszwolf, J. J. Multiphase monolith reactors: Chemical reaction engineering of segmented flow in microchannels. *Chem. Eng. Sci.* **2005**, *60*, 5895−5916.
(58) You, L.; Liu, H. A two-phase flow and transport model for the cathode of PEM fuel cells. *Int. J. Heat Mass Transfer* **2002**, *45*, 2277−2287.

DOI: 10.1021/acs.langmuir.8b03323
Langmuir 2019, 35, 3194−3203